Earth and Planetary Science Letters 531 (2020) 115971

Contents lists available at ScienceDirect

Earth and Planetary Science Letters

www.elsevier.com/locate/epsl

Sulfide-bearing cumulates in deep continental arcs: The missing copper reservoir

Kang Chen [a,b,*], Ming Tang [b], Cin-Ty A. Lee [b], Zaicong Wang [a,c], Zongqi Zou [a,c], Zhaochu Hu [a,c], Yongsheng Liu [a,c]

[a] State Key Laboratory of Geological Processes and Mineral Resources, China University of Geosciences, Wuhan 430074, China
[b] Department of Earth, Environmental and Planetary Sciences, Rice University, Houston, TX 77005, United States
[c] School of Earth Sciences, China University of Geosciences, Wuhan 430074, China

ARTICLE INFO

Article history:
Received 26 July 2019
Received in revised form 13 November 2019
Accepted 14 November 2019
Available online 26 November 2019
Editor: T.A. Mather

Keywords:
Cu-Ag
sulfide saturation
cumulate
continental arc
crust formation

ABSTRACT

Resolving the geochemical discrepancies between the bulk continental crust and its building blocks, basaltic arc magmas, can provide insights into the processes by which the continental crust is formed. One of the discrepancies is that the bulk continental crust is depleted in Cu and has a lower Cu/Ag ratio (∼500) than basaltic arc magmas (∼3500). How arc magmas become Cu-depleted and where the missing Cu resides remain unclear. Here, we report Cu and Ag concentrations in Arizona garnet-pyroxenite xenoliths, which represent cumulates formed in a deep continental arc. Many of these cumulates are Cu-enriched, with Cu concentrations as high as ∼1000 ppm. Furthermore, for the first time, we show that these cumulates have higher Cu/Ag ratios (up to ∼10,000) than basaltic arc magmas, complementary to the low Cu/Ag in felsic arc magmas and the continental crust (≤500). In these cumulates, Cu and Ag concentrations are initially low, but begin to rise with progressive differentiation due to sulfide saturation when cumulate Mg# (atomic ratio of Mg/(Mg+Fe)) decreases to ∼0.7. The onset of sulfide saturation in the cumulates is accompanied by a Cu decrease in continental arc magmas. Fractional crystallization modelling shows that the early sulfide saturation during the differentiation of continental arc magmas was facilitated principally by cooling and iron depletion in the melt. Our findings suggest that most of the Cu extracted from the mantle in continental arc settings is sequestered in sulfides in deep arc cumulates during magma differentiation. The sulfide-bearing cumulates represent the missing reservoir with both high Cu concentrations and high Cu/Ag ratios. The low Cu abundance and low Cu/Ag ratio in the average continental crust requires the formation of sulfide-bearing cumulate layer at arc roots followed by its delamination into the mantle. Moreover, we confirm that sulfide saturation in continental arc magmas occurs earlier (at higher Mg#) than in island arc settings, resulting in lower Cu concentrations in the felsic upper crust of continental arcs. Because the bulk continental crust is strongly depleted in Cu, these observations together point to syn-magmatic crustal thickening as a key process in making continents.

1. Introduction

Basaltic arc magmas generated in subduction zones are widely thought to be the building blocks of the continental crust (Taylor, 1977; Kelemen, 1995; Rudnick, 1995; Hawkesworth and Kemp, 2006), although other models of continent growth have also been suggested (e.g., the oceanic plateau model by Albarède, 1998). However, there are some geochemical discrepancies between the bulk continental crust and the basaltic arc magmas (e.g., Kelemen, 1995; Rudnick, 1995). Theses discrepancies suggest that something important is missing in our understanding of how continental crust forms. One of these discrepancies is that the estimated Cu abundance in the bulk continental crust (Rudnick and Gao, 2003 and references therein; Hu and Gao, 2008; Gaschnig et al., 2016; Chen et al., 2019) is significantly lower than in arc basalts and mid-ocean ridge basalts (MORB, Fig. 1a). Instead, Cu abundance of the average continental crust is more reminiscent of evolved magmas in continental arc settings. Reconciling this apparent deficit in Cu may provide critical insights into the differentiation mechanisms responsible for making the continental crust (Lee et al., 2012; Chiaradia, 2014; Jenner, 2017; Wang et al., 2018). Because of Cu's strong affinity for sulfide, it is thought that Cu is scavenged out of the magmas during differentiation by sulfide segregation

* Corresponding author at: State Key Laboratory of Geological Processes and Mineral Resources, China University of Geosciences, 388 Lumo Road, Hongshan District, Wuhan City, Hubei Province, 430074, China.
E-mail address: kangchen@cug.edu.cn (K. Chen).

https://doi.org/10.1016/j.epsl.2019.115971
0012-821X/

(Lee et al., 2012; Chiaradia, 2014; Jenner, 2017; Wang et al., 2018), a hypothesis that infers the existence of Cu-enriched cumulates in arc roots. However, evidence for such Cu-enriched cumulates has so far only been tentatively demonstrated on cumulates from one locality, the Sierra Nevada in California (Lee et al., 2012). And because the data is limited, the nature of the sulfide fractionation is still largely unknown (Lee et al., 2012).

In addition to Cu, Ag is also a strongly chalcophile element, but the two elements have different preferences for sulfide. Silver and Cu have the same partition coefficients (D) between liquid sulfide and silicate melt ($D_{Cu}/D_{Ag} = 1$), but different D values between crystalline sulfides and silicate melts with Cu being more compatible in crystalline sulfides than Ag ($D_{Cu}/D_{Ag} > 1$, All the D values used in this study are those between silicate melts and liquid/crystalline sulfides with a pyrrhotite composition) (Li and Audétat, 2012; Kiseeva and Wood, 2015). Their different D values make Cu/Ag ratio a valid tracer of crystalline versus liquid sulfide fractionation (Jenner et al., 2010; 2015; Wang et al., 2018; Cox et al., 2019). The bulk silicate earth (BSE), fertile mantle peridotites, MORB and primitive arc-related magmas have identical Cu/Ag ratios (∼3500, Fig. 1b), indicating limited crystalline sulfide fractionation during mantle partial melting and basaltic differentiation. The fact that the continental crust has lower Cu/Ag ratio than arc basalts requires an additional reservoir with high Cu/Ag ratio. However, no Ag data, to the best of knowledge, have currently been reported for deep arc cumulates (e.g., the Sierran cumulates from Lee et al. (2012)), and the high Cu/Ag reservoir, to date, has not been observed.

Here, we investigate garnet-pyroxenite xenoliths from Arizona, USA. Similar to those from Sierra Nevada (Lee et al., 2006; 2012), these xenoliths represent deep-seated cumulates that crystallized at the base of continental arc roots (Erdman et al., 2016; Tang et al., 2018; 2019a). Therefore, these samples may provide direct constraints to test the hypothesis that there is a Cu-enriched layer in deep arc. Comparing with the Sierran garnet-pyroxenite xenoliths, the Arizona xenoliths are much fresher and more abundant which represent a more comprehensive record of deep arc differentiation process. While the Cu concentrations in Sierra Nevada cumulates are scattered (Lee et al., 2012), systematic Cu trend along with Mg# in the Arizona cumulates (see section 4.2) is observed, which is useful to constrain the nature of sulfide saturation. In addition to our analyses of Cu, we also investigate the behavior of Ag. We show that many of these cumulates have high Cu concentrations and high Cu/Ag ratios that can balance the Cu-depleted and low Cu/Ag felsic arc magmas and bulk continental crust. We build on the approach by Lee et al. (2012) but explore a new approach to tease out the nature of sulfide fractionation. Moreover, we use Cu systematics to evaluate the redox conditions under which these sulfide-bearing cumulates might have formed. Our results have implications not just for deep crustal recycling, but also for how continents grow.

2. Samples

The Tertiary potassic latites from Camp Creek and Sullivan Buttes on the southwestern margin of the Colorado Plateau (central Arizona, USA) host numerous garnet-pyroxenite xenoliths (Esperanca and Holloway, 1984; Smith et al., 1994; Erdman et al., 2016), providing a rare opportunity to study deep crustal magmatic differentiation. We investigated 37 garnet-pyroxenite xenoliths from the collection of Erdman et al. (2016). These Arizona garnet-pyroxenite xenoliths are composed of variable proportions of garnet and clinopyroxene, with minor phases including amphibole, spinel, rutile, sulfide, apatite and titanite (Erdman et al., 2016), similar to those reported from Sierra Nevada (Lee et al., 2006). Pressure estimates showed that these garnet-pyroxenites crystallized at 45-80 km (Smith et al., 1994; Erdman et al., 2016) and their geochemical compositions are also similar to those reported as continental arc-related lower crustal cumulates from the Sierra Nevada batholith to the west (Lee et al., 2006). Selected major and trace element concentration data, mineral mode abundances, as well as titanite U-Pb ages for these samples have been reported by Erdman et al. (2016) and Erdman and Lee (2018). Additional geochemical data are reported in the following papers: Tang et al., 2018 (rare-earth elements in garnets and clinopyroxenes) and Tang et al., 2019a (Nb and Ta in whole rocks and rutiles).

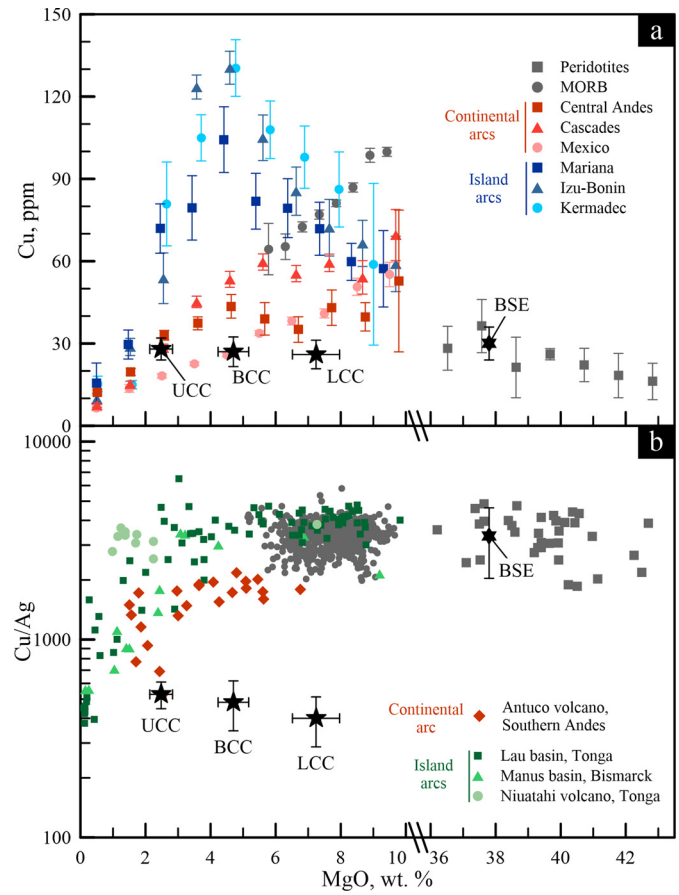

Fig. 1. (**a**) Copper versus MgO for peridotites, MORB, and arc-related magmas. Data are binned by 1% MgO content, and within each bin, the mean Cu concentration and two standard errors are plotted. Note the contrasting Cu-MgO paths between island arcs and continental arcs. The continental crust is depleted in Cu compared to primitive arc magmas and MORBs. Data sources: bulk silicate earth (BSE) and fertile peridotites from Wang and Becker (2015), MORB from Jenner and O'Neill (2012) and Yang et al. (2018), magmas from continental arcs (Central Andes, Cascades and Mexico) and island arcs (Mariana, Izu-Bonin and Kermadec) compiled from GEOROC (http://georoc.mpch-mainz.gwdg.de/georoc/Entry.html). (**b**) Cu/Ag ratio versus MgO for fertile peridotites, MORB and arc-related magmas. The Cu/Ag ratio is constant (3000-4000) in BSE, fertile peridotites, MORB and arc basalts, but significantly lower in felsic arc magmas and the continental crust (∼500). Data sources: Antuco volcano, Southern Andes from Cox et al. (2019), Manus basin, Bismarck arc from Jenner et al. (2010), Lau basin, Tonga arc from Jenner et al. (2012; 2015) and Niuatahi volcano, Tonga arc from Wang et al. (2019). Estimates for bulk, upper and lower continental crusts (denoted by BCC, UCC and LCC, respectively) in both (**a**) and (**b**) are from Rudnick and Gao (2003).

3. Analytical techniques

Whole rock Cu and Ag concentrations were measured using isotope dilution at the State Key Laboratory of Geological Processes and Mineral Resources, China University of Geosciences, Wuhan. Ten-100 g fresh rock samples were crushed and powdered in a ceramic SPEX mill placed in a shatterbox for 5-10 minutes per

Table 1
Copper and Ag concentrations in garnet-pyroxenite cumulates from Arizona and reference materials.

Sample	SiO_2[a]	TiO_2	Al_2O_3	FeO_{total}	MnO	MgO	CaO	Na_2O	K_2O	P_2O_5	LOI	Mg#	Cu (ppm)	Ag (ppb)	Cu/Ag
Arizano garnet-pyroxenite cumulates															
CC-ME1	49.5	0.173	7.58	8.04	0.25	15.0	17.5	0.441	0.038	0.022	1.1	0.77	48.2	8.94	5388
CC-ME2	43.2	3.47	13.3	15.6	0.24	9.82	12.2	1.06	0.15	0.52	0.47	0.53	54.9	31.7	1735
CC-ME4	40.7	2.39	16.4	15.2	0.33	5.74	15.4	0.794	0.12	0.38	1.2	0.40	163	14.8	11053
CC-ME8	48.2	0.904	10.7	9.04	0.12	13.1	16.0	0.881	0.17	0.062	1.5	0.72	58.0	23.9	2431
CC-ME11	43.5	1.07	13.8	13.5	0.26	12.2	11.5	1.50	0.71	0.14	1.0	0.62	53.6	22.6	2367
CC-ME14	43.0	2.18	13.8	13.6	0.17	12.5	11.4	1.53	0.64	0.013	1.3	0.62	123	36.0	3430
CC-ME16	43.1	2.83	16.9	13.9	0.23	10.3	12.0	0.718	0.086	0.041	0.57	0.57	25.6	16.7	1531
PR-62-DS	44.3	0.307	16.9	12.5	0.35	12.8	12.5	0.508	0.048	0.021	0.38	0.65	26.5	11.5	2314
PR-63-DS	41.8	1.25	15.8	15.4	0.14	10.0	10.1	2.05	1.6	0.23	0.92	0.54	22.8	43.0	530
PR-78-DS	44.4	1.39	15.3	15.5	0.30	8.49	12.7	1.53	0.083	0.025	0.12	0.49	225	29.6	7587
PRS-40-DS	51.1	0.569	6.28	7.38	0.09	13.0	19.9	1.31	0.012	0.008	0.65	0.76	5.05	15.8	320
Replicate													5.84	15.4	379
PRS-43-DS	51.3	0.481	6.14	7.09	0.11	13.7	20.1	1.05	0.016	0.012	0.55	0.78	17.7	15.1	1177
Replicate													14.5	15.1	960
PRT-5E-DS	43.8	1.68	13.8	16.7	0.31	8.71	12.8	1.45	0.19	0.051	0.53	0.48	51.8	19.0	2735
SB1-ME1	47.7	0.613	5.03	13.3	0.20	12.8	16.2	1.25	0.17	0.96	1.0	0.63	1017	111	9178
SB1-ME3	48.2	0.896	8.79	10.7	0.16	10.8	18.5	1.14	0.053	0.029	1.4	0.64	624	70.1	8897
Replicate													618	70.6	8754
SB1-ME7	44.2	1.06	15.3	12.3	0.19	7.87	15.5	1.04	0.23	0.021	1.4	0.53	410	58.9	6965
SB1-ME9	50.5	0.172	9.28	5.13	0.12	13.2	19.3	0.728	0.15	0.025	1.5	0.82	11.0	12.2	906
Replicate													12.2	11.6	1052
SB1-ME10	48.1	0.663	9.59	12.1	0.25	12.6	14.1	1.16	0.12	0.018	1.8	0.65	554	68.7	8070
SB1-ME11	50.2	0.578	7.37	11.0	0.22	16.5	12.3	0.776	0.16	0.009	1.5	0.73	105	22.2	4703
SB1-ME14	44.9	1.78	13.6	14.0	0.26	8.76	14.3	1.36	0.083	0.11	0.70	0.53	103	34.8	2959
SB1-ME16	45.6	0.711	13.3	13.5	0.26	11.1	12.9	1.18	0.19	0.026	0.86	0.59	125	42.5	2934
SB1-ME18	45.6	1.51	13.4	14.7	0.24	8.88	12.8	1.42	0.23	0.031	1.3	0.52	360	69.0	5223
SB1-ME21	48.3	0.638	9.63	11.1	0.24	13.7	13.6	1.02	0.27	0.035	1.3	0.69	391	48.2	8122
SB3-40-DS	43.6	1.42	15.1	15.0	0.23	9.24	13.7	1.33	0.33	0.087	0.65	0.52	162	30.4	5334
SB3-ME2	41.0	4.09	17.6	16.2	0.39	8.10	11.4	0.868	0.12	0.036	0.21	0.47	343	32.0	10702
SB3-ME5	42.9	1.84	13.8	16.8	0.33	8.12	12.6	1.56	0.19	0.12	0.62	0.46	181	32.1	5638
SB3-ME14	47.8	0.905	9.19	14.5	0.32	13.4	12.3	1.09	0.17	0.061	0.59	0.62	41.6	16.3	2543
SB3-ME19	41.4	1.92	15.7	17.5	0.31	8.67	10.7	1.80	0.61	0.12	1.0	0.47	80.7	35.7	2262
SB3-ME21	47.8	0.514	10.2	10.4	0.24	14.6	13.4	0.872	0.23	0.011	1.3	0.71	146	33.2	4392
SB3-ME25	38.5	3.53	17.1	19.8	0.34	6.88	11.7	0.493	0.16	1.6	0.04	0.38	72.2	7.02	10292
SB3-ME30	40.4	2.91	18.2	15.3	0.29	8.65	11.3	1.28	0.36	0.41	0.79	0.50	212	38.3	5536
SB3-ME31	44.1	1.58	14.7	15.5	0.31	8.22	14.3	1.15	0.07	0.083	0.45	0.49	66.0	15.2	4347
SB3-ME32	44.1	0.936	14.1	15.5	0.43	8.45	14.8	1.14	0.05	0.071	0.47	0.49	25.2	7.64	3303
SB3-ME37	48.2	0.774	8.17	13.4	0.26	16.0	11.3	0.782	0.19	0.020	0.23	0.68	250	32.2	7776
SB3-ME39	46.4	0.542	13.8	9.90	0.22	13.3	15.0	0.727	0.11	0.019	0.65	0.70	15.1	12.6	1197
Replicate													14.6	12.3	1187
SB3-ME40	49.3	0.530	8.30	11.3	0.24	15.0	13.4	0.896	0.48	0.022	1.0	0.70	149	35.0	4244
SB4-1-DS	43.6	2.33	14.6	15.6	0.37	8.07	13.7	1.02	0.18	0.017	1.4	0.48	12.8	10.9	1181
Reference materials															
UB-N_1													24.9	45.3	
UB-N_2													26.1	43.7	
Recommended values[b]													23 ± 2	45 ± 2	
BHVO_1													133	43.7	
BHVO_2													128	44.4	
BHVO_3													131	44.1	
Recommended values[b]													129 ± 1	44.5 ± 0.8	

[a] Major elements are from Erdman and Lee (2018).
[b] Recommended values are from Wang et al. (2015).

sample. Detailed procedures for powder digestion, ion exchange chromatography and instrumentation closely followed Wang et al. (2015). Briefly, ~0.1 g sample powder and ^{65}Cu-^{109}Ag spikes were digested using HNO_3-HF mixture in a Teflon Parr bomb and then aqua regia in a 15 mL PFA vial. For chemical separation, two columns were used: Column A, 2 mL AG1-X8 anion exchange resin, and Column B, 1 mL AG1-X8 anion exchange resin. Two fractions, containing Cu and Ag, respectively, were obtained after Column A separation. The Ag fraction was ready for ICP-MS measurements. The Cu fraction was further purified using Column B, and the final Cu solution was ready for ICP-MS measurements.

Isotopic ratios were measured on a sector field ICP-MS (Element XR, Thermo Fisher, Bremen, Germany) with an electron multiplier detector. The ICP-MS was fitted with a Twinnabar cyclonic spray chamber (*Glass Expansion*) and a 0.1 mL/min MicroMist Ezy-Fit nebulizer (*Glass Expansion*). To resolve Ti oxide interferences, the ^{65}Cu/^{63}Cu ratios were measured at a medium-resolution mode ($m/\Delta m = 4000$). The ^{109}Ag/^{107}Ag ratios were determined at a low-resolution mode. The ^{91}Zr and ^{93}Nb were monitored because of their potential oxide interferences on Ag. These oxide interferences are negligible in our measurements, indicative of effective purification, thus no correction was made. Three total procedural blanks were analyzed during the whole analyses campaign, yielding averages of 12 ng Cu and 30 pg Ag, respectively. Blank corrections were made for all samples. The blank contributions are <1% for Cu and <2% for most Ag measurements. Reference materials UB-N (serpentinite) and BHVO-2 (basalt) were analyzed as unknowns along with the Arizona cumulates. As shown in Table 1, our results are in good agreement with published values. Five replicates were analyzed, and the five samples were replicated well (Table 1).

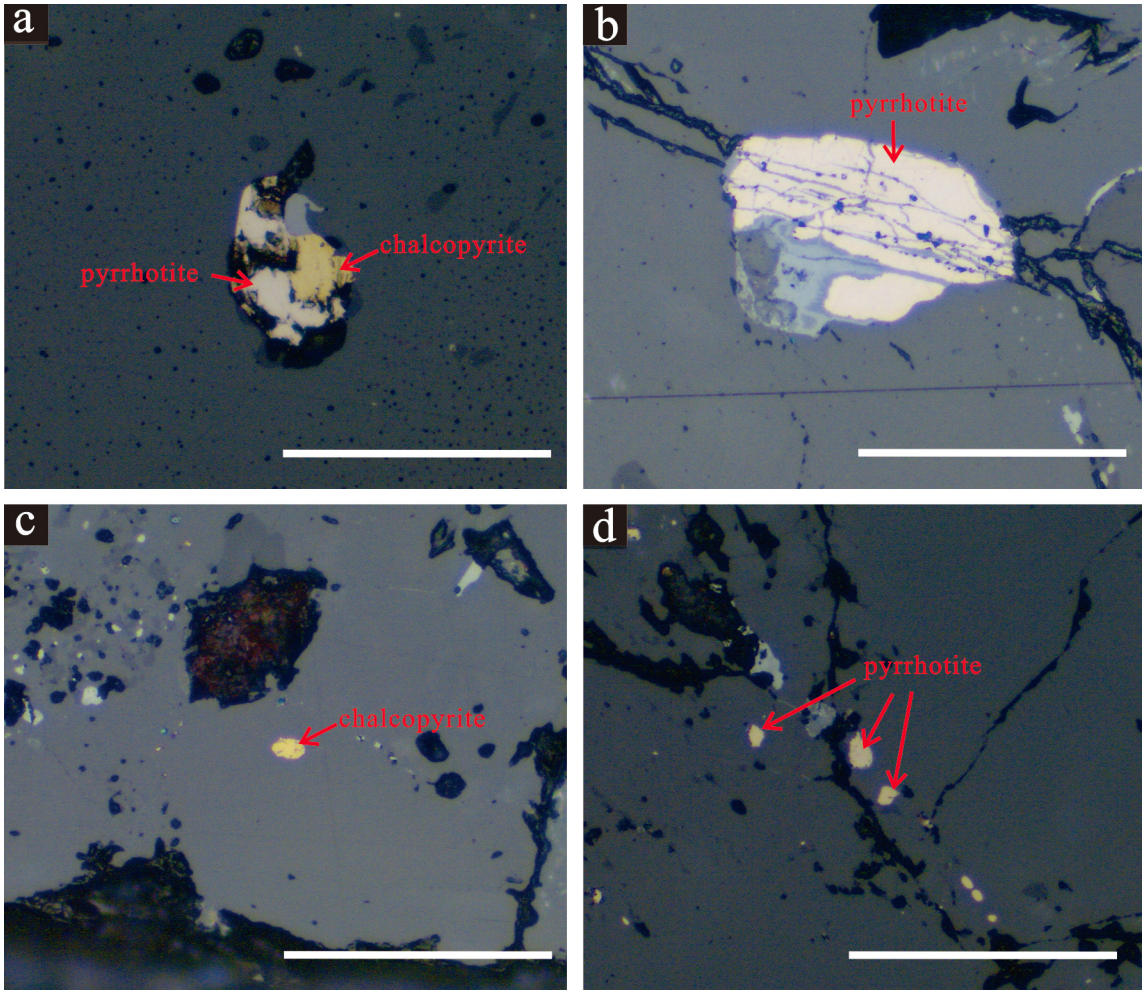

Fig. 2. Sulfides in the Arizona garnet-pyroxenite cumulates. **a**: Irregularly shaped pyrrhotite and chalcopyrite inclusions. **b**: Intergranular pyrrhotite showing incipient alteration along edges and fractures. **c**: An angular chalcopyrite inclusion. **d**: Irregularly shaped pyrrhotite inclusions. In our samples, irregular sulfides are dominated by pyrrhotites existing as magmatic sulfide inclusions in garnets and clinopyroxenes, like those shown in **d**. Occasionally, intergranular pyrrhotites like the one presented in **b** are also observed. And most of the intergranular pyrrhotites are oxidized along edges and fractures. Chalcopyrite inclusions (**c**) and polymineralic inclusions composed of pyrrhotite and chalcopyrite (**a**) are rare. Insets **a** and **b** are from sample SB1-ME1, and **c** and **d** are from sample SB1-ME3. White scale bars are 100 μm.

4. Results

4.1. Sulfides

Chalcophile elements are mainly concentrated in sulfides owing to their high D between sulfide and silicate phases (Li and Audétat, 2012; Kiseeva and Wood, 2015). In our samples, sulfides are dominated by pyrrhotite and mainly occur as magmatic sulfide inclusions in garnets and clinopyroxenes (Figs. 2a, c and d). Occasionally, intergranular sulfides are observed (Fig. 2b) and very small sulfides (<5 μm) exist in the cores of oxides. Some magmatic sulfide inclusions in garnets or clinopyroxenes occur as polymineralic inclusions composed of pyrrhotite and chalcopyrite (Fig. 2a), while others occur as singe phases of chalcopyrite (Fig. 2c) or pyrrhotite (Fig. 2d). They show variable sizes (from <1 to ∼50 μm) and irregular or angular shapes (Figs. 2a, c and d). The presence of these magmatic sulfides in many of the cumulates suggests that sulfide saturation was achieved during magma differentiation.

4.2. Cu and Ag concentrations

Both whole-rock Cu and Ag show a triangular distribution pattern when plotted versus whole rock Mg# in the cumulates (Fig. 3a, b). Their concentrations are low in the most primitive cumulates of Mg# > 0.75 (stage 1), then increase with decreasing Mg# until Mg# reaches ∼0.60 (stage 2), after which both Cu and Ag concentrations decline with decreasing Mg# (stage 3). Most of the Arizona cumulates have higher Cu concentrations than the estimates of average bulk continental crust of ∼27 ppm (BCC). The highest Cu concentration is ∼1000 ppm. Most of the samples have Ag concentration lower than the BCC. Unlike Cu, Ag is probably not depleted during magmatic differentiation due to the lower D_{Ag} in crystalline sulfides (∼30) than D_{Cu} (Li and Audétat, 2012; Kiseeva and Wood, 2015; Cox et al., 2019). The difference between D_{Cu} and D_{Ag} in crystalline sulfides is also shown in the Cu/Ag versus Mg# plot (Fig. 3c). Excluding the samples with Cu and/or Ag concentrations lower than MORB (as their Cu/Ag may be affected by silicates and trapped melts), these cumulates show overall increasing Cu/Ag ratios with decreasing Mg# in stages 2 and 3 (Fig. 3c).

5. Discussion

5.1. A cumulate origin for Arizona garnet-pyroxenites

Four lines of evidence imply a cumulate origin for these garnet-pyroxenites. First, there are obvious magmatic, cumulate textures in some of the samples (Erdman et al., 2016). Second, their major element concentrations are similar to the cumulates derived from experimental studies of high pressure, hydrous fractionation (Müntener and Ulmer, 2018 and references therein) (Fig. 4a). The

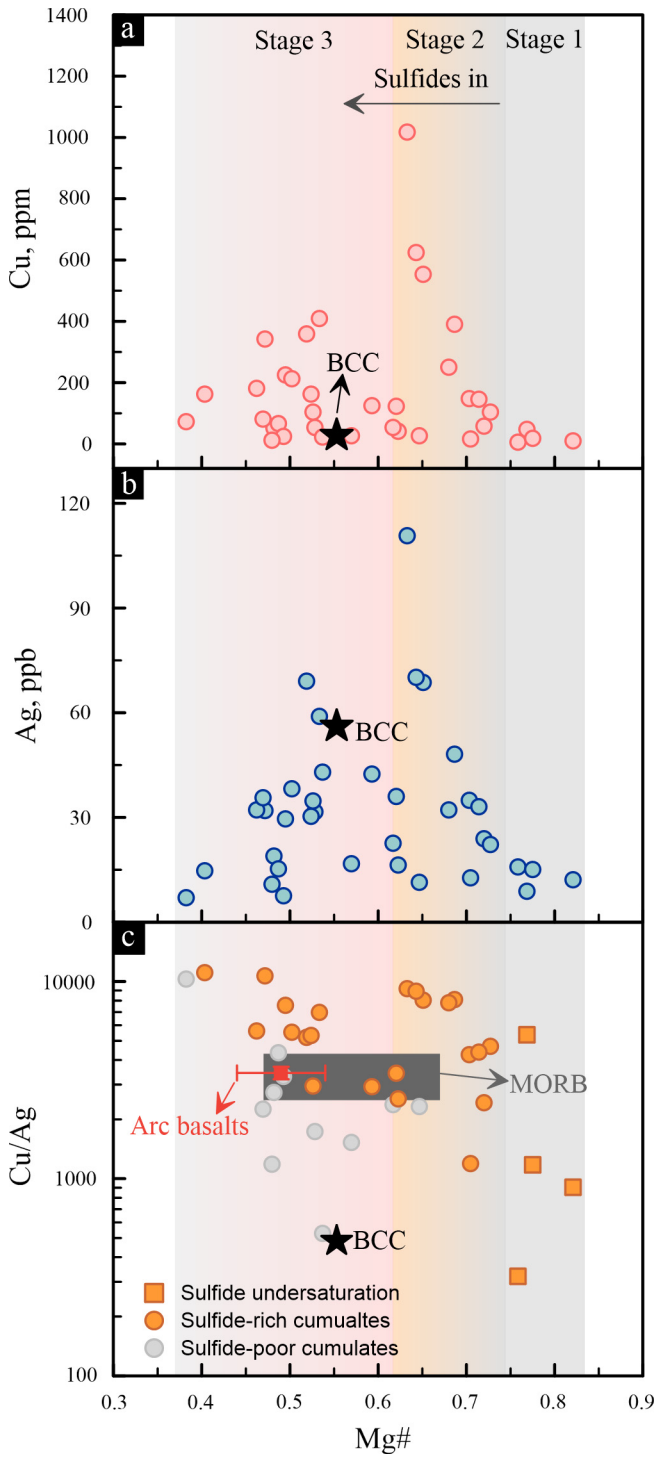

Fig. 3. Cu (**a**), Ag (**b**), Cu/Ag (**c**) versus Mg# in the Arizona garnet-pyroxenite cumulates. The areas with brighter colors in stages 2 and 3 mean higher sulfide mode in the cumulates, as suggested by the higher Cu concentrations. The sulfide-rich and sulfide-poor cumulates after sulfide saturation in (**c**) are divided based on the concentrations of Cu and Ag concentrations relative to those of primitive MORB (Mg# > 0.80) (90 ppm and 27 ppb) (Jenner and O'Neill, 2012; Yang et al., 2018). Data sources for arc basalts (SiO_2 < 54%), MORB and the bulk continental crust (BCC, the star) are the same as in Fig. 1. (For interpretation of the colors in the figure(s), the reader is referred to the web version of this article.)

Arizona garnet-pyroxenites represent the middle segment of the "Z-shaped" cumulate line of descent, displaying a decrease of SiO_2 along with a quick drop of Mg# largely due to the fractionation of garnets which are depleted in Si and enriched in Fe (dominated by almandine in the Arizona samples). Third, the garnet-pyroxenite xenoliths show identical major element compositions to those from Sierra Nevada, which are of cumulate origin (Lee et al., 2006), and to the cumulates from Kohistan arc (Jagoutz et al., 2006; Dhuime et al., 2007). Finally, the increasing FeO_T trend with decreasing Mg# in the Arizona samples is complementary to the calc-alkaline differentiation trends in the Sierra Nevada batholith and Central Andes magmas marked by strong Fe depletion (Fig. 4b) (Chin et al., 2018; Lee et al., 2018; Tang et al., 2019a).

5.2. Tracking sulfide saturation during magma differentiation

In this section, we use Cu and Ag systematics to shed light on the nature of sulfide fractionation during differentiation. We divide magma differentiation into three stages based on the Cu and Ag systematics in the Arizona cumulates. The first stage corresponds to cumulate Mg# > 0.75 (melt Mg# >∼0.63, see Appendix B), during which the Cu and Ag concentrations in the Arizona cumulates are low, similar to (for Cu) or lower (for Ag) than their abundances in the average bulk continental crust. Because Cu and likely Ag are highly incompatible in silicate minerals (Lee et al., 2012; Liu et al., 2014), the low Cu and Ag concentrations in the most primitive cumulates suggest no sulfide saturation in the initial basaltic differentiation. The second stage starts with the rapid increase in Cu and Ag concentrations with decreasing Mg# between 0.75 and 0.60 as a result of sulfide fractionation. As differentiation proceeds, the residual magma eventually reaches sulfide saturation. Sulfide fractionation scavenges highly chalcophile elements (e.g., Cu) from the melt and enriches the cumulates with these elements. The third stage is marked by decreasing Cu and Ag concentrations with decreasing Mg# at Mg# < 0.60. At this stage, the system remains sulfide saturated as evidenced by the overall high Cu and Ag concentrations in the cumulates, but the amount of crystallizing sulfides declines along the liquid line of descent. We emphasize that the foregoing discussion reflects general trends. In detail, there are individual samples that do not follow these general trends. For example, several samples from the second and the third stages have anomalously low Cu and Ag. Clearly, other processes, such as melt-rock reaction and magmatic recharge (Lee et al., 2006), may complicate the signals, but it is the overall trends that are of interest to us in this paper.

We now turn to the Cu/Ag ratios of the cumulates. While Cu and Ag elemental concentrations may index the onset of sulfide saturation, Cu/Ag ratio can potentially be used to determine what types of sulfides are fractionated, liquid or crystalline sulfides. Liquid sulfide has D_{Cu}/D_{Ag} of ∼1 whereas crystalline sulfides have $D_{Cu}/D_{Ag} > 1$. Therefore, crystalline sulfides can fractionate Cu from Ag but liquid sulfide cannot. During the stage 1, the system is under-saturated in sulfides, so the cumulates have very low Cu and Ag concentrations and their fractionation is controlled by silicate minerals and trapped melt. After sulfide saturation (stage 2 and 3), cumulate Cu/Ag ratio generally increases with decreasing Mg# (Fig. 3c), which is consistent with sulfide fractionation transitioning from liquid sulfide (= melt Cu/Ag) to crystalline sulfide (> melt Cu/Ag), presumably as a result of cooling. Collectively, these cumulates record a differentiation series from sulfide undersaturated to liquid sulfide saturated and finally to crystalline sulfide saturated.

5.3. Modelling sulfide fractionation in continental arc magma differentiation

In magmatic systems, sulfide solubility is a function of pressure, temperature, melt composition and oxygen fugacity (fO_2) (Wallace and Carmichael, 1992; O'Neill and Mavrogenes, 2002; Liu et al., 2007; Li and Ripley, 2009; Jugo et al., 2010; Ariskin et al., 2013;

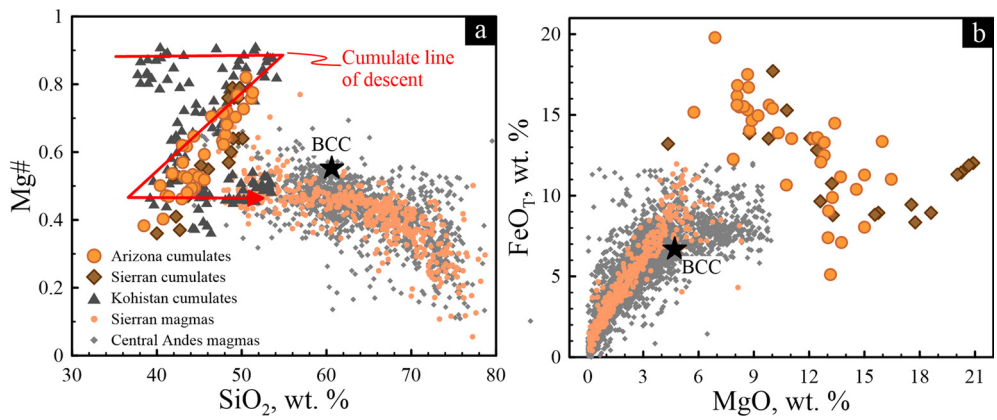

Fig. 4. Mg# versus SiO_2 (**a**) and FeO_T versus MgO (**b**) in deep arc cumulates and Sierra Nevada batholith and Central Andes, which belong to the calc-alkaline magma series, as indicated by the FeO_T depletion trends. The Arizona xenoliths plot on an identical trend to those of the cumulates from Sierra Nevada, Kohistan arc and the cumulate line of descent from experiment work (**a**). The Arizona xenoliths are also complementary to the Fe depleting calc-alkaline magma differentiation series (**b**). Data sources are as follows: major elements for the Arizona cumulates from Erdman et al. (2016), the cumulates and the magmas from Sierra Nevada from Lee et al. (2006; 2018), the cumulate line of descent (the Z-shaped trend, hydrous differentiation sequence from basaltic melts under 1-1.5 GPa) from Müntener and Ulmer (2018), Kohistan arc cumulates from Jagoutz et al. (2006) and Dhuime et al. (2007), Central Andes magmas from GEOROC (http://georoc.mpch-mainz.gwdg.de/georoc/Entry.html), and bulk continental crust (BCC) from Rudnick and Gao (2003).

Fortin et al., 2015; Smythe et al., 2017). In particular, because sulfur can exist in both S^{2-} and S^{6+} in silicate melts (e.g., Jugo et al., 2005; 2010), magma redox conditions can have profound influence on sulfide saturation and thus the fate of chalcophile elements like Cu and Ag.

5.3.1. Model assumptions

We now model sulfide fractionation during continental arc magma differentiation. Our calculation couples the empirical equations of sulfur content at sulfide saturation (SCSS) with a continuous fractional crystallization model. Because the Arizona garnet-pyroxenites represent the deep arc cumulates from calc-alkaline magmas, we use igneous rocks from Central Andes as an empirical way to constrain the melt compositions during differentiation. The pressure range is constrained by the Arizona cumulates (Smith et al., 1994; Erdman et al., 2016) and the temperature is estimated using pMELTS (Ghiorso et al., 2002).

There are a number of published SCSS models (Wallace and Carmichael, 1992; O'Neill and Mavrogenes, 2002; Li and Ripley, 2009; Ariskin et al., 2013; Smythe et al., 2017), but only the SCSS models from Liu et al. (2007) and Fortin et al. (2015) were calibrated over a temperature range most relevant to our model. We use the SCSS model from Fortin et al. (2015) as it represents an updated version of the model from Liu et al. (2007). It is worth pointing out that the SCSS model from Fortin et al. (2015) does not consider the effect of sulfide composition. Adding of Ni and/or Cu into a pure FeS phase has been shown to lower the SCSS (Ariskin et al., 2013; Smythe et al., 2017). For example, adding 10% Cu into a pure FeS phase would decrease SCSS by ~100 ppm relative to a pure FeS (Smythe et al., 2017). This ~100 ppm difference would not change the model results significantly and thus the effect of sulfide composition on SCSS will not be considered in the following discussion. The Cu concentration of the initial magma (Mg# = 0.7) is assumed to be ~50 ppm based on primitive continental arc magmas (Fig. 1a) and the initial S concentration was suggested to be 800-1000 ppm modelled from a 10% degree melting of a mantle peridotite with ~200 ppm S (Lee et al., 2012; Ding and Dasgupta, 2017).

The details of the model assumptions and calculations can be found in Appendix A. A spreadsheet is also provided for the calculation procedures in Appendix B. The main assumptions are as follows:

1. We use a compilation of Central Andes igneous rocks to quantify the liquid lines of descent for calc-alkaline differentiation series from Mg# of 0.7 to 0.2. We assume that the water content increases linearly from 4 wt. % to 8 wt. % with differentiation.

2. We let pressure decrease linearly from 2 GPa at Mg# = 0.7 to 1 GPa at Mg# = 0.2. More details on this assumption can be found in Appendix A. Melt temperature is calculated by pMELTS (Ghiorso et al., 2002) for each composition.

3. We use the SCSS model by Fortin et al. (2015) to obtain the S^{2-} solubility in the melt and the empirical equation from Jugo et al. (2010) to calculate the total S content for any given melt fO_2.

4. The mass fraction (F) of the residual magma in each step relative to the initial magma is calculated using K_2O contents, which we treat as a near perfectly incompatible element so that residual melt fraction is the inverse of the K_2O enrichment relative to the parental magma. We divide the fractionated phases into two groups: sulfides and non-sulfide minerals. Initial S content in the melt is 1000 ppm and S is assumed to be perfectly incompatible in non-sulfide minerals. The partition coefficients for Cu is ~1000 between liquid sulfide and silicate melt, and ~300 between crystalline sulfide and silicate melts. To use these partition coefficients, we assume the sulfide phases have a pyrrhotite composition. This is because, for an immiscible sulfide melt equilibrating with a silicate melt with Cu and Ni existing as trace elements, the sulfide melt usually has a pyrrhotite composition (Li and Audétat, 2012; Kiseeva et al., 2017). Chalcopyrite or pentlandite may be formed in local environments when Cu or Ni becomes very enriched. Moreover, Cu-sulfides in the Arizona cumulates are rare and most of the sulfides present in the cumulates are pyrrhotite. When the temperature is >1200°C, liquid sulfide dominates, and at temperature <1200°C, crystalline sulfide is the major sulfide phase (Zhang and Hirschmann, 2016). Silicate minerals have a bulk Cu partition coefficient of 0.05.

5. We consider two possible fO_2 evolution paths during magma differentiation. First, the fO_2 is assumed to be constant during magma differentiation. Second, the fO_2 is assumed to increase linearly by two logarithmic units as magma Mg# decreases from 0.7 to 0.2 (Tang et al., 2018; 2019b; Lee and Tang, 2020, see below for details).

5.3.2. Sulfide fractionation under constant melt fO_2

Our model results at constant fO_2 are shown in Fig. 5. At fO_2 below FMQ (fayalite-magnetite-quartz oxygen fugacity buffer), SCSS is independent of fO_2 (e.g., O'Neill and Mavrogenes, 2002), because S^{2-} is the dominant S species. The calculated initial SCSS (melt Mg# = 0.70) is ~1380 ppm, higher than the S content in

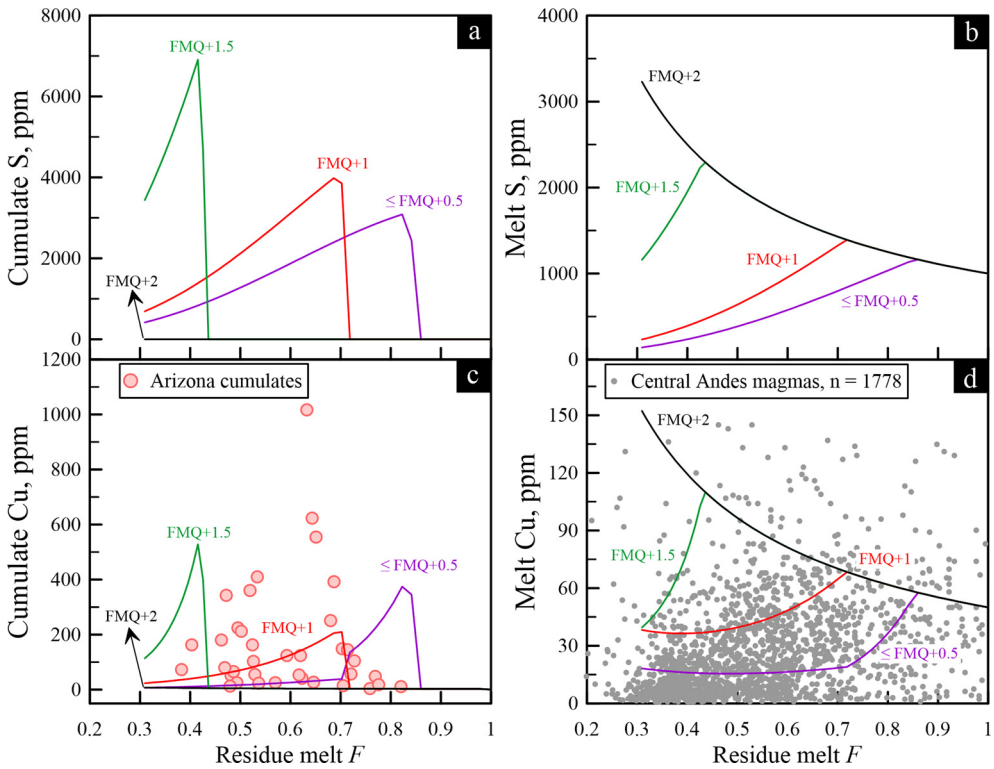

Fig. 5. Calculated S and Cu concentrations in cumulates and residual melt as a function of melt fraction F with constant melt fO_2 during continental arc magma differentiation. When fO_2 is above FMQ+2, sulfide remains undersaturated in the entire differentiation process. To produce the Cu trends seen in the Arizona cumulates and continental arc magmas, fO_2 must be < FMQ+0.5. Data for Central Andes magmas are compiled from GEOROC. And the residual melt F for Central Andes magmas are calculated using the same method from the modelling (please see the fourth assumption in Section 5.3.1).

the initial melt (∼1000 ppm). Thus, the melt is undersaturated initially, and the S and Cu concentrations will increase in the residual melt and are negligible in the cumulates (Fig. 5a and c). As differentiation proceeds, the SCSS decreases, due to decreasing T and decreasing melt FeO_T content (O'Neill and Mavrogenes, 2002; Smythe et al., 2017), and the melt will eventually reach sulfide saturation. Copper concentration in the instantaneous cumulate increases rapidly after sulfide saturation (Fig. 5c), and then decreases as the melt becomes Cu depleted. At fO_2 < FMQ+0.5, our model can produce simultaneously the Cu systematics seen in continental arc magmas and Arizona cumulates. The Cu peak in cumulates become extremely narrow under slightly oxidized conditions (fO_2 = FMQ+1.5, Fig. 5c). At fO_2 > FMQ+2, sulfides remain undersaturated throughout the differentiation because most of the S is oxidized to S^{6+}, thus the high SCSS (Jugo et al., 2005). In this case, Cu behaves as an incompatible element and its concentration in the melt continues increasing with differentiation (Fig. 5d).

5.3.3. Sulfide fractionation under increasing melt fO_2

Recently, it has been suggested that magma oxygen fugacity may increase with differentiation in continental arcs built on thick crust due to the fractionation of garnet, which has high total Fe contents but low $Fe^{3+}/\sum Fe$ (Tang et al., 2018; 2019b). To explore this effect in a simple manner, we assume the melt fO_2 increases linearly by two log units during the entire differentiation process, the lower bound of the fO_2 increase from Tang et al. (2018). We find that, under increasing melt fO_2, the initial melt fO_2 must be lower than FMQ to saturate sulfides during differentiation (Fig. 6). In fact, an even lower initial melt fO_2 (<FMQ-0.5) is required to generate the continuous Cu depletion along the liquid line of descent seen in continental arc magmas (Figs. 6d and 1a).

5.3.4. Uncertainties and caveats

The largest uncertainty in our modelling is the redox window of S^{2-}-S^{6+} transition. We used the empirical melt $S^{6+}/\sum S - fO_2$ relationship from Jugo et al. (2010), which was obtained for a basaltic system at 0.2 GPa and 1050 °C. The recent work by Matjuschkin et al. (2016) and Nash et al. (2019) showed that both temperature and pressure can affect the melt $S^{6+}/\sum S - fO_2$ relationship such that S^{2-}-S^{6+} transition occurs at lower fO_2 at higher temperature and lower pressure. We did not parameterize the temperature and pressure effects in our modelling in part because these effects have not been calibrated experimentally. Using the $S^{6+}/\sum S - fO_2$ relationship from Jugo et al.'s (2010) low pressure experiments (0.2 GPa) may underestimate the fO_2 of S^{2-}-S^{6+} transition at the higher pressures assumed in our modelling (1-2 GPa). However, the temperature of the onset of sulfide saturation in our modelling is also higher (∼1200°C) than in Jugo et al.'s (2010) experiments (1050°C). Thus, the temperature and pressure effects on S^{2-}-S^{6+} transition and sulfide saturation may largely compensate each other. Although our modelling suggests that the fO_2 of the primitive arc magma is likely reduced (<FMQ), the pressure effect on S^{2-}-S^{6+} transition, which is not accounted for in our model, may allow sulfide saturation under oxidized conditions if the differentiation pressure is sufficiently high (Matjuschkin et al., 2016). Thus, the current modelling does not allow for precise constraint on the redox condition of the primitive arc magmas. Indeed, some previous studies suggested that the primitive arc magmas may be oxidized, caused by oxidized fluids released from subducted slab (e.g., Kelley and Cottrell, 2009). Additionally, our simplified model cannot precisely quantify the timing and amount of sulfide fractionation because of the uncertainties in SCSS and S^{2-}-S^{6+} transition and the complexities associated with continental arc differentiation processes, but our model can reproduce the overall Cu trends in both cumulates and continental arc magmas (Figs. 5 and 6).

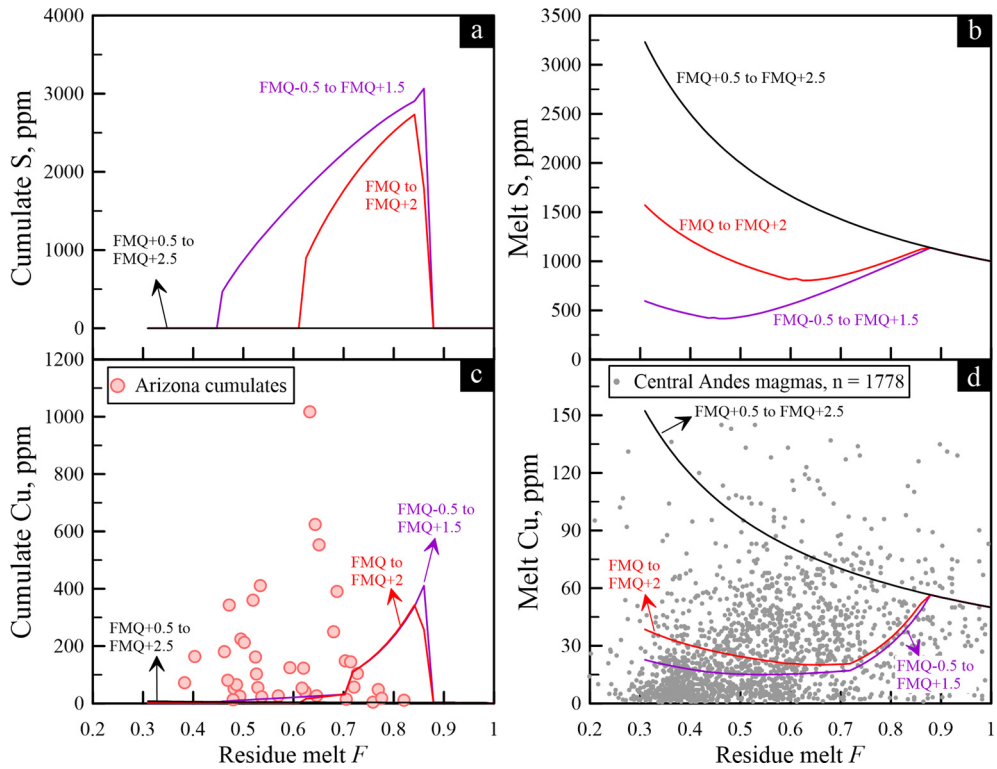

Fig. 6. Calculated S and Cu concentrations in cumulates and residual melts with increasing fO_2 during differentiation. When the initial fO_2 is above FMQ+0.50, sulfide will remain undersaturated through the entire differentiation process. Sulfide saturation can be achieved when the initial fO_2 is $\leq$ FMQ. To produce the Cu trends in the Arizona cumulates and continental arc magmas, the initial fO_2 must be $\leq$ FMQ-0.5. Results for the initial fO_2 < FMQ-0.5 are similar to those for the initial fO_2 = FMQ-0.5. Data for Central Andes magmas are the same as in Fig. 5.

5.4. Implications for continental crust formation

The Arizona garnet-pyroxenite cumulates are, to the best of our knowledge, the first rocks that have been reported so far to show significantly higher Cu/Ag ratios than the primitive arc magmas and MORB. Together with their high Cu concentrations, these cumulates may represent the missing reservoir with both high Cu concentration and high Cu/Ag ratios to balance the low Cu concentration and low Cu/Ag ratios of evolved arc magmas (Fig. 7a). It has been suggested that 80-95% of the modern continental crust was generated in subduction zones (Barth et al., 2000; Hawkesworth and Kemp, 2006) and the modern continental crust is characterized by depleted Cu and low Cu/Ag ratio (Rudnick and Gao, 2003). To obtain a bulk continental crust with low Cu abundance and low Cu/Ag ratio requires the formation of a high Cu concentration and high Cu/Ag cumulate layer in arc roots followed by its recycling into the mantle (Fig. 7) (Lee et al., 2012; Jenner, 2017; Wang et al., 2018). The geochemical mismatch between the basaltic crustal building blocks and the modern andesitic continental crust, also referred to as the "crust composition paradox", leads to the long-standing hypothesis of a missing ultramafic reservoir, but the nature of this missing reservoir remains enigmatic (e.g., Rudnick, 1995; Lee, 2014). Our work here suggests that a large amount of Cu sequestered in sulfides is recycled back into the mantle together with the delaminated mafic-ultramafic rocks.

Importantly, a comparison of the Cu concentrations in continental arcs, island arcs and the average continental crust indicates that not all subduction zones may generate the magma differentiation series that fits the continental crust compositions (Fig. 1). Today, island arc magmas are systematically more enriched in Cu than continental arc magmas (Chiaradia, 2014). Island arc magmas with MgO >$\sim$ 3% have Cu concentrations much higher than the average continental crust (50-130 ppm versus $\sim$30 ppm). By contrast, Cu

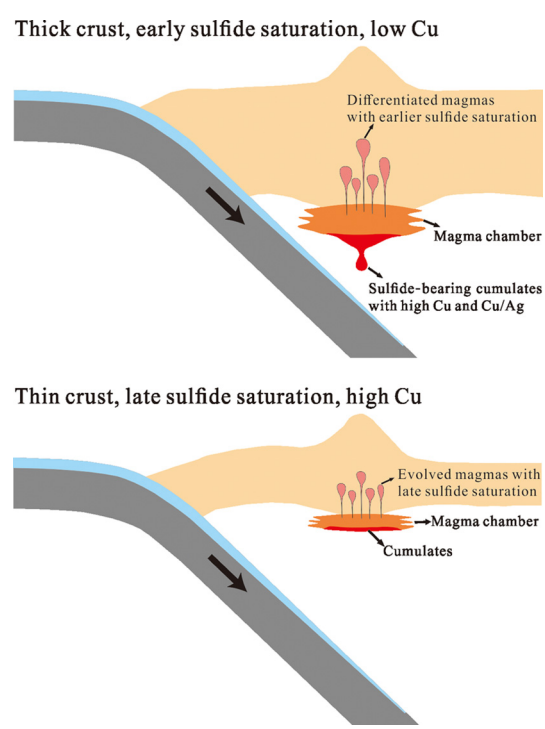

Fig. 7. Cartoon showing the timing of sulfide saturation during magma differentiation in thick arcs versus thin arcs. Early fractionation of sulfides at the roots of thick arcs (e.g., continental arcs) sequesters Cu from the magmas. These sulfides, together with the mafic-ultramafic rocks, may be recycled back into the mantle, driving the Cu depletion of the bulk continental crust. The relatively late sulfide saturation in the magmas of thin arcs (e.g., island arcs) results in higher Cu concentration in thin arc crust than in the bulk continental crust.

concentrations in continental arc magmas decrease gradually from ∼50 ppm to ∼10 ppm with differentiation, with the bulk continental crust lying within the trend (Fig. 1a). These observations require early sulfide saturation, as is the case in continental arcs, in making continental crust (Fig. 7) (Jenner, 2017; Lee and Tang, 2020). Thus syn-magmatic crustal thickening is critical for making the continental crust. This viewpoint is consistent with the complementary Nb/Ta systematics observed in cumulates and magmas formed in continental arcs (Tang et al., 2019a), which also indicates that the continental crust predominantly formed in magmatic orogens such as thick continental arcs.

6. Conclusions

The lower Cu abundance and lower Cu/Ag ratio in the bulk continental crust than its building blocks, basaltic arc magmas, implies that something is missing for the Cu budget during mantle-crust differentiation. Garnet-pyroxenites from Arizona, USA, which represent deep-seated cumulates from an extinct continental arc, were analyzed for Cu and Ag concentrations by isotope dilution. The Arizona cumulates are sulfide-bearing and enriched in Cu (up to ∼1000 ppm). And they also have higher Cu/Ag (up to ∼10,000) than arc basalts. Copper and Ag systematics in the Arizona cumulates and continuous Cu depletion in continental arc magma differentiation suggest earlier sulfide saturation than in island arc magmas. Modelling shows that the earlier sulfide saturation is facilitated by cooling and iron depletion in the melt.

Two major implications can be drawn from the above observations and calculations. One is that most of the Cu extracted from the mantle in continental arc settings is scavenged by sulfides in deep cumulates during magma differentiation. The low Cu abundance and low Cu/Ag ratio in the average continental crust requires the formation of Cu-enriched cumulate layers at arc roots followed by its recycling into the mantle (delamination/foundering). The other is that, to achieve a Cu-depleted continental crust, continent growth should mainly occur in thick continental arcs, rather in thin island arcs. Therefore, syn-magmatic crustal thickening is a necessary step for making continents.

Declaration of competing interest

The authors declare that they have no known competing financial interests or personal relationships that could have appeared to influence the work reported in this paper.

Acknowledgements

This work was supported by the National Natural Science Foundation of China (41703034, 41973024), the 111 Project from Chinese Ministry of Education (BP0719022), and the State Key Laboratory of Geological Processes and Mineral Resources (MSFGPMR12, MSFGPMR02-1). Ming Tang is grateful for the support from U.S. National Science Foundation (EAR-1850832). Yinuo Liu and Tao He are thanked for the help on isotope dilution analyses. We thank John Mavrogenes and Massimo Chiaradia for their constructive reviews and Tamsin Mather for the editorial handling and insightful comments.

Appendix A. Supplementary material

Supplementary material related to this article can be found online at https://doi.org/10.1016/j.epsl.2019.115971.

References

Albarède, F., 1998. The growth of continental crust. Tectonophysics 296 (1–2), 1–14.
Ariskin, A.A., Danyushevsky, L.V., Bychkov, K.A., McNeill, A.W., Barmina, G.S., Nikolaev, G.S., 2013. Modeling solubility of Fe-Ni sulfides in basaltic magmas: the effect of nickel. Econ. Geol. 108 (8), 1983–2003.
Barth, M.G., McDonough, W.F., Rudnick, R.L., 2000. Tracking the budget of Nb and Ta in the continental crust. Chem. Geol. 165 (3–4), 197–213.
Chen, K., Rudnick, R.L., Wang, Z., Tang, M., Gaschnig, R.M., Zou, Z., He, T., Hu, Z., Liu, Y., 2019. How mafic was the Archean upper continental crust? Insights from Cu and Ag in ancient glacial diamictites. Geochim. Cosmochim. Acta. https://doi.org/10.1016/j.gca.2019.08.002. In press.
Chiaradia, M., 2014. Copper enrichment in arc magmas controlled by overriding plate thickness. Nat. Geosci. 7 (1), 43–46.
Chin, E.J., Shimizu, K., Bybee, G.M., Erdman, M.E., 2018. On the development of the calc-alkaline and tholeiitic magma series: a deep crustal cumulate perspective. Earth Planet. Sci. Lett. 482, 277–287.
Cox, D., Watt, S.F.L., Jenner, F.E., Hastie, A.R., Hammond, S.J., 2019. Chalcophile element processing beneath a continental arc stratovolcano. Earth Planet. Sci. Lett. 522, 1–11.
Dhuime, B., Bosch, D., Bodinier, J.L., Garrido, C.J., Bruguier, O., Hussain, S.S., Dawood, H., 2007. Multistage evolution of the Jijal ultramafic-mafic complex (Kohistan, N Pakistan): implications for building the roots of island arcs. Earth Planet. Sci. Lett. 261 (1–2), 179–200.
Ding, S., Dasgupta, R., 2017. The fate of sulfide during decompression melting of peridotite – implications for sulfur inventory of the MORB-source depleted upper mantle. Earth Planet. Sci. Lett. 459, 183–195.
Erdman, M.E., Lee, C.-T.A., 2018. Whole rock composition data for garnet pyroxenites from Arizona. IEDA. https://doi.org/10.1594/IEDA/111138.
Erdman, M.E., Lee, C.-T.A., Levander, A., Jiang, H., 2016. Role of arc magmatism and lower crustal foundering in controlling elevation history of the Nevadaplano and Colorado Plateau: a case study of pyroxenitic lower crust from central Arizona, USA. Earth Planet. Sci. Lett. 439, 48–57.
Esperanca, S., Holloway, J.R., 1984. Lower crustal nodules from the Camp Creek Latite, Carefree, Arizona. In: Kornprobst, J. (Ed.), Developments in Petrology. Elsevier, pp. 219–227.
Fortin, M.-A., Riddle, J., Desjardins-Langlais, Y., Baker, D.R., 2015. The effect of water on the sulfur concentration at sulfide saturation (SCSS) in natural melts. Geochim. Cosmochim. Acta 160, 100–116.
Gaschnig, R.M., Rudnick, R.L., McDonough, W.F., Kaufman, A.J., Valley, J.W., Hu, Z., Gao, S., Beck, M.L., 2016. Compositional evolution of the upper continental crust through time, as constrained by ancient glacial diamictites. Geochim. Cosmochim. Acta 186, 316–343.
Ghiorso, M.S., Hirschmann, M.M., Reiners, P.W., Kress, V.C., 2002. The pMELTS: a revision of MELTS for improved calculation of phase relations and major element partitioning related to partial melting of the mantle to 3 GPa. Geochem. Geophys. Geosyst. 3 (5), 1–35.
Hawkesworth, C.J., Kemp, A.I.S., 2006. Evolution of the continental crust. Nature 443 (7113), 811–817.
Hu, Z., Gao, S., 2008. Upper crustal abundances of trace elements: a revision and update. Chem. Geol. 253 (3–4), 205–221.
Jagoutz, O., Müntener, O., Burg, J.P., Ulmer, P., Jagoutz, E., 2006. Lower continental crust formation through focused flow in km-scale melt conduits: the zoned ultramafic bodies of the Chilas Complex in the Kohistan island arc (NW Pakistan). Earth Planet. Sci. Lett. 242 (3), 320–342.
Jenner, F.E., 2017. Cumulate causes for the low contents of sulfide-loving elements in the continental crust. Nat. Geosci. 10 (7), 524–529.
Jenner, F.E., O'Neill, H.S.C., 2012. Analysis of 60 elements in 616 ocean floor basaltic glasses. Geochem. Geophys. Geosyst. 13 (2), Q02005.
Jenner, F.E., O'Neill, H.S.C., Arculus, R.J., Mavrogenes, J.A., 2010. The magnetite crisis in the evolution of arc-related magmas and the initial concentration of Au, Ag and Cu. J. Petrol. 51 (12), 2445–2464.
Jenner, F.E., Arculus, R.J., Mavrogenes, J.A., Dyriw, N.J., Nebel, O., Hauri, E.H., 2012. Chalcophile element systematics in volcanic glasses from the northwestern Lau Basin. Geochem. Geophys. Geosyst. 13 (6), Q06014.
Jenner, F.E., Hauri, E.H., Bullock, E.S., König, S., Arculus, R.J., Mavrogenes, J.A., Mikkelson, N., Goddard, C., 2015. The competing effects of sulfide saturation versus degassing on the behavior of the chalcophile elements during the differentiation of hydrous melts. Geochem. Geophys. Geosyst. 16 (5), 1490–1507.
Jugo, P.J., Luth, R.W., Richards, J.P., 2005. An experimental study of the sulfur content in basaltic melts saturated with immiscible sulfide or sulfate liquids at 1300°C and 1.0 GPa. J. Petrol. 46 (4), 783–798.
Jugo, P.J., Wilke, M., Botcharnikov, R.E., 2010. Sulfur K-edge XANES analysis of natural and synthetic basaltic glasses: implications for S speciation and S content as function of oxygen fugacity. Geochim. Cosmochim. Acta 74 (20), 5926–5938.
Kelemen, P., 1995. Genesis of high Mg# andesites and the continental crust. Contrib. Mineral. Petrol. 120 (1), 1–19.
Kelley, K.A., Cottrell, E., 2009. Water and the oxidation state of subduction zone magmas. Science 325 (5940), 605–607.
Kiseeva, E.S., Wood, B.J., 2015. The effects of composition and temperature on chalcophile and lithophile element partitioning into magmatic sulphides. Earth Planet. Sci. Lett. 424, 280–294.
Kiseeva, E.S., Fonseca, R.O.C., Smythe, D.J., 2017. Chalcophile elements and sulfides in the upper mantle. Elements 13 (2), 111–116.

Lee, C.T.A., 2014. 4.12 - physics and chemistry of deep continental crust recycling. In: Holland, H.D., Turekian, K.K. (Eds.), Treatise on Geochemistry, second edition. Elsevier, Oxford, pp. 423–456.

Lee, C.-T.A., Tang, M., 2020. How to make porphyry copper deposits. Earth Planet. Sci. Lett. 529, 115868.

Lee, C.-T.A., Cheng, X., Horodyskyj, U., 2006. The development and refinement of continental arcs by primary basaltic magmatism, garnet pyroxenite accumulation, basaltic recharge and delamination: insights from the Sierra Nevada, California. Contrib. Mineral. Petrol. 151 (2), 222–242.

Lee, C.-T.A., Luffi, P., Chin, E.J., Bouchet, R., Dasgupta, R., Morton, D.M., Le Roux, V., Yin, Q.-z., Jin, D., 2012. Copper systematics in arc magmas and implications for crust-mantle differentiation. Science 336 (6077), 64–68.

Lee, C.-T.A., Erdman, M., Yang, W., Ingram, L., Chin, E.J., DePaolo, D.J., 2018. Sulfur isotopic compositions of deep arc cumulates. Earth Planet. Sci. Lett. 500, 76–85.

Li, Y., Audétat, A., 2012. Partitioning of V, Mn, Co, Ni, Cu, Zn, As, Mo, Ag, Sn, Sb, W, Au, Pb, and Bi between sulfide phases and hydrous basanite melt at upper mantle conditions. Earth Planet. Sci. Lett. 355–356, 327–340.

Li, C., Ripley, E.M., 2009. Sulfur contents at sulfide-liquid or anhydrite saturation in silicate melts: empirical equations and example applications. Econ. Geol. 104 (3), 405–412.

Liu, Y., Samaha, N.-T., Baker, D.R., 2007. Sulfur concentration at sulfide saturation (SCSS) in magmatic silicate melts. Geochim. Cosmochim. Acta 71 (7), 1783–1799.

Liu, X., Xiong, X., Audétat, A., Li, Y., Song, M., Li, L., Sun, W., Ding, X., 2014. Partitioning of copper between olivine, orthopyroxene, clinopyroxene, spinel, garnet and silicate melts at upper mantle conditions. Geochim. Cosmochim. Acta 125, 1–22.

Matjuschkin, V., Blundy, J.D., Brooker, R.A., 2016. The effect of pressure on sulphur speciation in mid- to deep-crustal arc magmas and implications for the formation of porphyry copper deposits. Contrib. Mineral. Petrol. 171 (7), 66.

Müntener, O., Ulmer, P., 2018. Arc crust formation and differentiation constrained by experimental petrology. Am. J. Sci. 318 (1), 64–89.

Nash, W.M., Smythe, D.J., Wood, B.J., 2019. Compositional and temperature effects on sulfur speciation and solubility in silicate melts. Earth Planet. Sci. Lett. 507, 187–198.

O'Neill, H.S.C., Mavrogenes, J.A., 2002. The sulfide capacity and the sulfur content at sulfide saturation of silicate melts at 1400°C and 1 bar. J. Petrol. 43 (6), 1049–1087.

Rudnick, R.L., 1995. Making continental crust. Nature 378 (6557), 571–578.

Rudnick, R.L., Gao, S., 2003. 3.01 - Composition of the continental crust. In: Holland, H.D., Turekian, K.K. (Eds.), Treatise on Geochemistry, 1st ed. Pergamon, Oxford, pp. 1–64.

Smith, D., Arculus, R.J., Manchester, J.E., Tyner, G.N., 1994. Garnet-pyroxene-amphibole xenoliths from Chino Valley, Arizona, and implications for continental lithosphere below the Moho. J. Geophys. Res., Solid Earth 99 (B1), 683–696.

Smythe, D.J., Wood, B.J., Kiseeva, E.S., 2017. The S content of silicate melts at sulfide saturation: new experiments and a model incorporating the effects of sulfide composition. Am. Mineral. 102 (4), 795–803.

Tang, M., Erdman, M., Eldridge, G., Lee, C.-T.A., 2018. The redox "filter" beneath magmatic orogens and the formation of continental crust. Sci. Adv. 4 (5).

Tang, M., Lee, C.-T.A., Chen, K., Erdman, M., Costin, G., Jiang, H., 2019a. Nb/Ta systematics in arc magma differentiation and the role of arclogites in continent formation. Nat. Commun. 10 (1), 235.

Tang, M., Lee, C.-T.A., Costin, G., Höfer, H.E., 2019b. Recycling reduced iron at the base of magmatic orogens. Earth Planet. Sci. Lett. 528, 115827.

Taylor, S.R., 1977. Island arc models and the composition of the continental crust. In: Talwani, M., Pitman, W.C. (Eds.), Island Arcs, Deep Sea Trenches and Back-Arc Basins.

Wallace, P., Carmichael, I.S.E., 1992. Sulfur in basaltic magmas. Geochim. Cosmochim. Acta 56 (5), 1863–1874.

Wang, Z., Becker, H., 2015. Abundances of Ag and Cu in mantle peridotites and the implications for the behavior of chalcophile elements in the mantle. Geochim. Cosmochim. Acta 160, 209–226.

Wang, Z., Becker, H., Wombacher, F., 2015. Mass fractions of S, Cu, Se, Mo, Ag, Cd, In, Te, Ba, Sm, W, Tl and Bi in geological reference materials and selected carbonaceous chondrites determined by isotope dilution ICP-MS. Geostand. Geoanal. Res. 39 (2), 185–208.

Wang, Z., Becker, H., Liu, Y., Hoffmann, E., Chen, C., Zou, Z., Li, Y., 2018. Constant Cu/Ag in upper mantle and oceanic crust: implications for the role of cumulates during the formation of continental crust. Earth Planet. Sci. Lett. 493, 25–35.

Wang, Z., Park, J.-W., Wang, X., Zou, Z., Kim, J., Zhang, P., Li, M., 2019. Evolution of copper isotopes in arc systems: insights from lavas and molten sulfur in Niuatahi volcano, Tonga rear arc. Geochim. Cosmochim. Acta 250, 18–33.

Yang, S., Humayun, M., Salters, V.J.M., 2018. Elemental systematics in MORB glasses from the mid-Atlantic ridge. Geochem. Geophys. Geosyst. 2018GC007593.

Zhang, Z., Hirschmann, M.M., 2016. Experimental constraints on mantle sulfide melting up to 8 GPa. Am. Mineral. 101 (1), 181–192.